AJNR

Three-Dimensional Multivoxel Proton MR Spectroscopy of the Brain in Children with Neurofibromatosis Type 1

Oded Gonen, Zhiyue J. Wang, A. Kasi Viswanathan, Patricia T. Molloy and Robert A. Zimmerman

AJNR Am J Neuroradiol 1999, 20 (7) 1333-1341
http://www.ajnr.org/content/20/7/1333

AJNR Am J Neuroradiol 20:1333–1341, August 1999

Three-Dimensional Multivoxel Proton MR Spectroscopy of the Brain in Children with Neurofibromatosis Type 1

Oded Gonen, Zhiyue J. Wang, A. Kasi Viswanathan, Patricia T. Molloy, and Robert A. Zimmerman

BACKGROUND AND PURPOSE: **Neurofibromatosis type 1 (NF1), the most common autosomal dominant genetic disorder, frequently manifests as focal areas of signal intensity (FASI) on T2-weighted MR images. The purpose of our study was to investigate whether tumor(s), focal areas of signal intensity (FASI), and normal brain can be differentiated by using 3D multivoxel localized proton MR spectroscopy in children with neurofibromatosis type 1 (NF1) disorder.**

METHODS: **Five children with NF1 and two healthy control subjects, all in the 3- to 11-year-old age group, were studied with a new 3D proton MR spectroscopy technique: a hybrid of 1D fourth-order transverse Hadamard spectroscopic imaging and 2D chemical shift imaging. A 3D volume-of-interest (VOI) was image-guided onto the site of the abnormality and identified on three orthogonal images. Proton MR spectroscopy partitioned the VOI into 6 × 6 × 4 (or 8 × 8 × 4) voxels, 1.5 (or 1.0) cm^3 each.**

RESULTS: **Simultaneous coverage of the entire VOI yielded good spectral signal-to-noise ratio from 136 (or 256) voxels in 27 minutes. Proton MR spectroscopy indicated that FASI a) are characterized by significantly elevated choline (Cho), reduced creatine (Cr), 2>Cho:Cr>1.3, and near normal *N*-acetylaspartate (NAA) levels; b) are different from tumors that exhibit Cho:Cr>2 and no NAA; c) have no intrinsic lipid or lactate signal(s); and d) correlate in spatial extent but are more extensive than indicated by MR imaging.**

CONCLUSION: **Three-dimensional multivoxel proton MR spectroscopy reveals distinct metabolic features that differentiate normal, FASI, and tumor regions in the pediatric brain.**

Neurofibromatosis type 1 (NF1) is the most frequent autosomal dominant genetic disease in humans, affecting one in 3000 to 4000 individuals, regardless of race, ethnic origin, or sex (1, 2). Although NF1 is considered a childhood neurocutaneous disorder, it has significant lifetime morbidity (3–6). Its most common neuroimaging features are focal areas of signal intensity (FASI) on T2-weighted MR images. Also known as hamartomas, or, less specifically, as unidentified bright objects, they are most often located in the basal ganglia, thalamus, cerebellum, and subcortical white matter (2, 6, 7). Low-grade brain stem and optic pathway glial tumors accompany FASI in about 20% of these cases (6). Unlike FASI of NF1, tumors expand the normal architecture of the structure within which they occur, a phenomenon known as mass effect (6, 8). While these tumors may or may not enhance with contrast administration, FASI are not known to do so (6, 8). Therefore, differentiating tumors from FASI depends on the ability to identify mass effect or enhancement or both in these lesions with current imaging techniques.

Although they are thought to represent sites of vacuolar or spongiotic changes (9), the range of NF1 lesions, from FASI to glial tumor, is not understood, nor has their heterogeneity been investigated. Since NF1 gene mutations may affect neuronal development, the metabolism of such regions is of clinical importance (10). Proton MR spectroscopy offers noninvasive metabolic assessment of these lesions, which, because they rarely undergo biopsy, are, in most cases, of unknown histopathologic origin (6–8). To evaluate combinations of diffuse FASI and tumors in multiple locations, 3D coverage around the entire region is needed. Given

Received January 22, 1998; accepted after revision March 11, 1999.

Supported by a Biomedical Technology Development grant from the Whitaker Foundation, by NIH grants NS33385 and NS37739, and by the U.S. Army Research and Development Command.

Center, Philadelphia, PA (O.G., A.K.V.); and the Department of Radiology, the Children's Hospital of Philadelphia (Z.J.W., P.T.M., R.A.Z.).

Address reprint requests to Oded Gonen, PhD, Division of Medical Science, Fox Chase Cancer Center, 7701 Burholme Ave, Philadelphia, PA 19111.

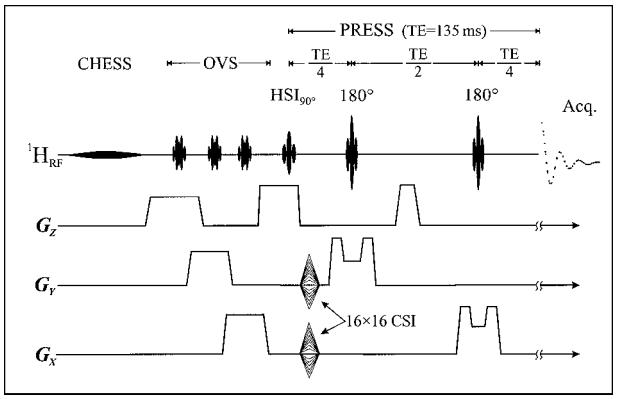

FIG 1. The hybrid 2D-CSI/1D-HSI sequence. A 25.6-millisecond 60-Hz CHESS sequence was followed by three 5.12-millisecond, dual-lobe, time-shifted $90+\varepsilon_i°$ (ε_i = 17°, 10°, and 5° to compensate for partial fat T1 recovery) OVS pulses. The VOI was selectively excited by a TR/TE = 1600/135 PRESS sequence with its 5.12-millisecond 90° pulse as well as fourth-order HSI encoding under a 3 mTM^{-1} gradient. This was followed 27.5 and 100 milliseconds later by a 5.12-millisecond 180° RF pulse under 1 mTM^{-1}. The 2D 16 × 16 CSI sequence was performed during the TE along the *x* and *y* axes.

the uncertainties associated with anatomic MR data, the question for MR spectroscopy is, How much of the disease process is tumor and how much surrounding tissue is sufficiently different metabolically to be distinguishable from it?

Currently, 3D proton MR spectroscopy in the brain is achieved by sequentially interleaving *N*, usually four, 2D slices (11–15). Unfortunately, this technique is inefficient in signal-to-noise ratio (SNR) per unit of time, since each slice is sampled only 1/N of the recycle time (TR) and spends (N − 1)/N of it idle. Consequently, reasonable voxel SNR from four such slices at 1.5 T requires 35 to 45 minutes, for a total examination time of approximately 90 minutes (12, 13, 16). This is a serious obstacle in pediatric applications, since children are usually sedated. Because MR spectroscopy comes late in the protocol, it is aborted if the sedation wears off, resulting in partial or total loss of the data. We address this difficulty with a 3D hybrid of 2D chemical shift imaging (CSI) and 1D fourth-order Hadamard spectroscopic imaging (HSI), shown in Figure 1. Coverage of the entire volume of interest (VOI) yielded in approximately half the time $\sqrt{2}$ better SNR than did four interleaves of equal TR, TE, and spectral and spatial resolution (17).

Methods

Patients and Control Subjects

Five children with NF1, ranging in age from 3 to 10 years, were examined with this hybrid technique. All were undergoing clinically indicated MR studies to which proton MR spectroscopy was added with parental informed consent. Patients younger than 7 years were sedated with pentobarbital sodium (6 mg/kg body weight, not to exceed 150 mg). MR spectroscopy was performed after the sagittal and coronal T1-weighted, axial T2- and proton density–weighted MR sequences and the T2-weighted fluid-attenuated inversion recovery sequences, but before injection of contrast material. This strategy was chosen to prevent underestimation of the levels of the choline (Cho)-containing metabolites (18). The control subjects, two boys, one 7 months old and one 11 years old, underwent the same MR spectroscopy protocol. They had been scheduled for MR imaging for reasons not related to NF1, and had no identifiable disease. Informed consent was obtained from their parents for the extra 30 minutes or so of MR spectroscopy. No sedation was needed for the 11-year-old child.

The 1D-HSI/2D-CSI Hybrid

CSI and HSI are complementary multivoxel localization methods (17, 19, 20). CSI is best for the long axes (eg, the anteroposterior [AP] and left-right [LR] directions) in the brain and HSI performs better along the short axes (ie, the inferosuperior [IS] direction). The hybrid, shown in Figure 1, combines them to exploit these individual strengths and to avoid their weaknesses (17, 19, 21). First, its 3D coverage yields an $\sqrt{N}$ SNR/unit-time advantage over *N* sequential interleaved 2D CSI slices. Second, the spatially selective HSI 90° pulse incorporates naturally into a point-resolved spectroscopy (PRESS) double spin-echo sequence (22) to localize and reject fat simultaneously (see Fig 1). Third, a VOI with one short and two long dimensions is required, at proton voxel sizes of approximately 1 mL; HSI is optimal for the former and CSI for the latter (11–15, 23, 24).

The position and size of the PRESS box and HSI partitions were interactively image-guided in three perpendicular planes using the manufacturer's software. Our custom IDL program (Research Systems, Boulder, CO) generated the shaped radiofrequency (RF) pulses shown in Figure 1: three 5-millisecond Outer Volume Suppression (OVS) dual-lobe sinc pulses, 30% time-shifted for reduced peak RF power; four 5-millisecond HSI pulses, representing the rows of the fourth-order Hadamard matrix, H_4; and two 5-millisecond refocusing 180° RF pulses in the complementary directions. The sequence has been described in detail elsewhere (17, 20).

Instrumentation

The experiments were done on a 1.5-T imaging unit using its standard circularly polarized head coil and actively shielded gradients. At approximately 10-Hz full-width at half-height water line, the magnetic field, B_0, homogeneity from the VOI was achieved with the manufacturer's auto-shim procedure in approximately 5 minutes. A single chemical-shift selective (CHESS) suppression pulse reduced the water signal approximately a hundredfold (25). Subcutaneous fat signals were suppressed more than 10^5 times by a combination of a) OVS in six planes containing the skull; b) selective VOI excitation with PRESS TR/TE = 1600/135, as shown in Figure 1 (11); c) destructive interference of residual signals in postprocessing by the add-subtract nature of the Hadamard transform; and d) T2 decay of the lipid signal during the 135 TE (17).

The proton MR spectroscopic data were processed off-line. A 2-Hz gaussian filter was applied to the FIDs, which were Fourier transformed in the temporal and in two spatial dimensions. Hadamard transform was applied in the third direction (19). No spatial filtering was applied.

Safety: RF Power Deposition

To assess the specific absorption rate (SAR), we assumed that most of the RF energy of the sinc pulses in Figure 1 was concentrated in the central lobe. Approximating it to a rectangular pulse of a duration equal to the inverse bandwidth, each OVS pulse deposited approximately 0.3 J and each PRESS pulse contributed approximately 1.2 J. Assuming approximately 2 kg for a child's head, the approximate 4.0 J

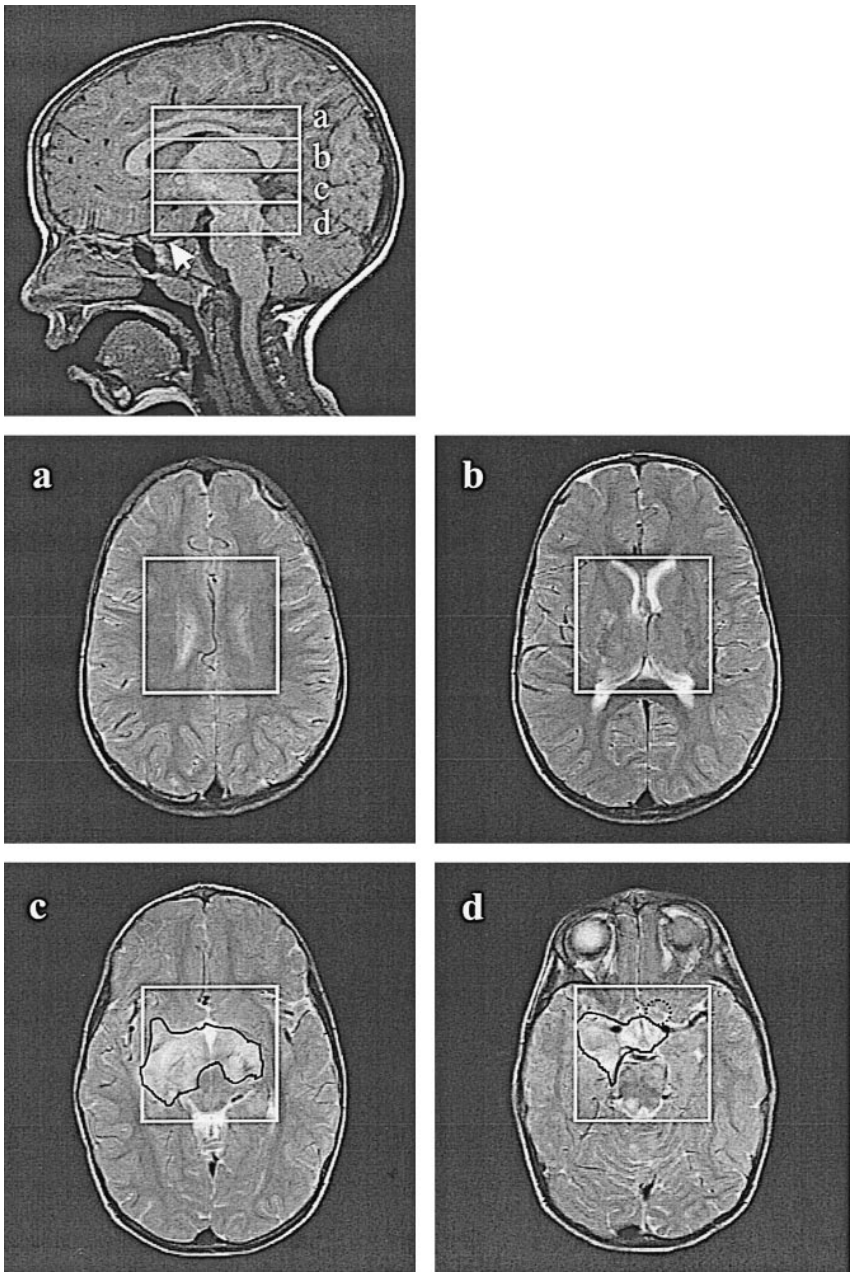

FIG 2. *Top,* Sagittal image shows the placement of the 6 × 6 × 6-cm PRESS VOI, the four 1.5-cm-thick HSI slices, *a–d,* and the chiasmal glioma (*arrow*) in a 3-year-old boy.

a–d, Axial T2-weighted images (FOV = 22 cm) of the corresponding HSI slices, superimposed with the axial projection of the 6 × 6-cm VOIs. The FASI regions were marked with a *solid black line* by a neuroradiologist. The *dotted circle* in *d* indicates the location of the glioma.

deposited at a TR of 1600 accrued approximately 1.25 $W \cdot kg^{-1}$, well under the FDA's 3.2 $W \cdot kg^{-1}$ SAR guidelines for the head. It is also within both the stricter 2 $W \cdot kg^{-1}$ guideline in the U.K. and the new international standard IEC 601–2–33 of 3 $W \cdot kg^{-1}$ over any 1-minute period.

Results

All five of the NF1 patients studied had brain tumors, four in the optic pathways and one in the brain stem. All had FASI in the basal ganglia, thalamus, brain stem, and even in the temporal lobe. The hybrid sequence of Figure 1 was applied to each with a $6_{AP} \times 6_{LR} \times 6_{IS}$-cm PRESS box image-guided onto the location of the lesions. It was partitioned with $16_{AP} \times 16_{LR}$ 2D CSI in the axial planes and fourth-order HSI along the IS direction. This produced four HSI slices, 36 voxels per slice, 1 × 1 × 1.5-cm each, for a total of 144 voxels in the PRESS box. A TR of 1600 was chosen to optimally match the 1000 to 1400 TR of the T1-weighted sequence for proton brain metabolites (26, 27) and the effective 90° PRESS nutation angle (26). The image-guided VOI positioning, shimming, and hybrid MR spectroscopy added approximately 35 minutes to the protocol, making the entire examination approximately 70 minutes long.

The MR images and MR spectra from two studies are presented in Figures 2 through 5. The PRESS box and HSI partitions, a through d, are superimposed on the sagittal images, Figures 2 and 4, and the axial MR images from the center of each HSI slice. A neuroradiologist traced the FASI on

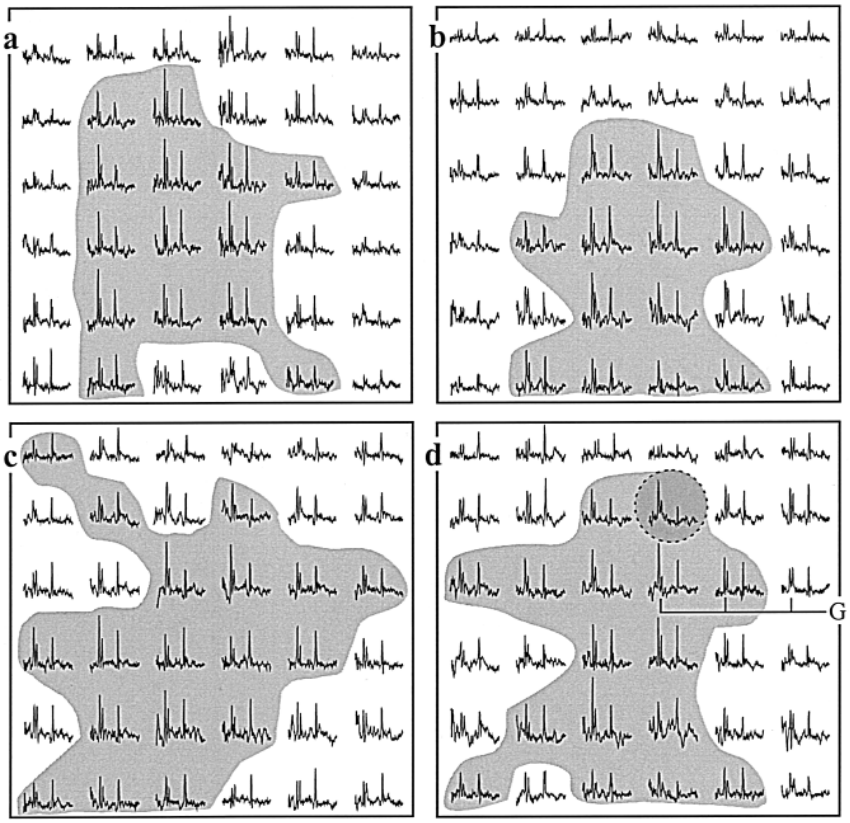

FIG 3. *a–d,* Real part of the proton spectra from the PRESS boxes on the corresponding images in Figure 2. The tumor spectrum in *d* is highlighted with a *dashed shaded circle,* and regions of elevated 2>Cho:Cr>1.3 are shaded. All spectra display the 4.0 to 0.5 ppm chemical shift range and are plotted on the same vertical scale, and each represents signal from a 1.5-cm^3 voxel.

the images before seeing the MR spectra. The proton spectra from HSI slices a through d of Figures 2 and 4 are shown in Figures 3 and 5, respectively. In each case, the spectra from the voxel(s) corresponding to the glioma on the MR images in Figures 2 and 4 are indicated by dashed, shaded circles. Note that these regions yield a high Cho:Cr>2 ratio, which is typical of tumors in children and adults (8, 28–31). Regions of elevated 2>Cho:Cr>1.3, which extend much farther then the tumorlike voxel(s) in each patient, were shaded by a spectroscopist before seeing the FASI outline on the MR image.

Two studies of healthy control subjects age-matched to the patients in Figures 2 and 4 were also conducted. Their results are shown for comparison in Figures 6 and 7, respectively, with the two slices closest in location to the unidentified bright objects/tumor in the corresponding patient displayed. The VOIs in these studies were slightly larger, 8 × 8 cm versus 6 × 6 cm in the axial planes for higher coverage, but shorter, ×4 cm compared with ×6 cm, along the IS direction. This resulted in smaller voxels, 1 cm^3 as opposed to 1.5 cm^3. All other experimental parameters were unchanged. The real part of the 8 × 8 proton spectra matrices from these studies is shown in Figures 6 and 7. They both reveal that the normal Cho:Cr ratio is approximately 1.0 ± 10% in brain regions similar to those investigated in the patients. The Cho:Cr ratio is, on average, slightly less than 1 for the 7-month-old and slightly exceeds unity, typical of the adult brain, in the 11-year-old.

Discussion

Recognition of what is and what is not a tumor depends on the ability of an imaging technique to differentiate mass effect from contrast enhancement. However, there are instances in which such differentiation is not possible, owing to a lack of either. In the two cases shown (see Figures 2 and 4), there are criteria to indicate by mass effect that a tumor is present. The question then becomes how much of the disease process seen is tumor and whether any surrounding tissue is sufficiently different from it. If so, the remaining possibility for that tissue is that it is an FASI. The 3D coverage, resolution, and SNR of proton MR spectroscopy shown here allow us to distinguish proton metabolic characteristics of tumor from FASI and normal brain. This is shown in Figure 3D, in which one, and in Figure 5c and d, in which two voxels display high Cho levels and near absence of any other metabolite, characteristic of both pediatric and adult brain tumors (8, 28–31). The tumorlike metabolite levels correlate with the 1 × 1-cm MR spectroscopy spatial resolution, with the known position and volume of these gliomas approximately 2 mL and 3 mL for these patients, respectively. The trace of NAA seen in the tumor voxel in Figure 3d is due to

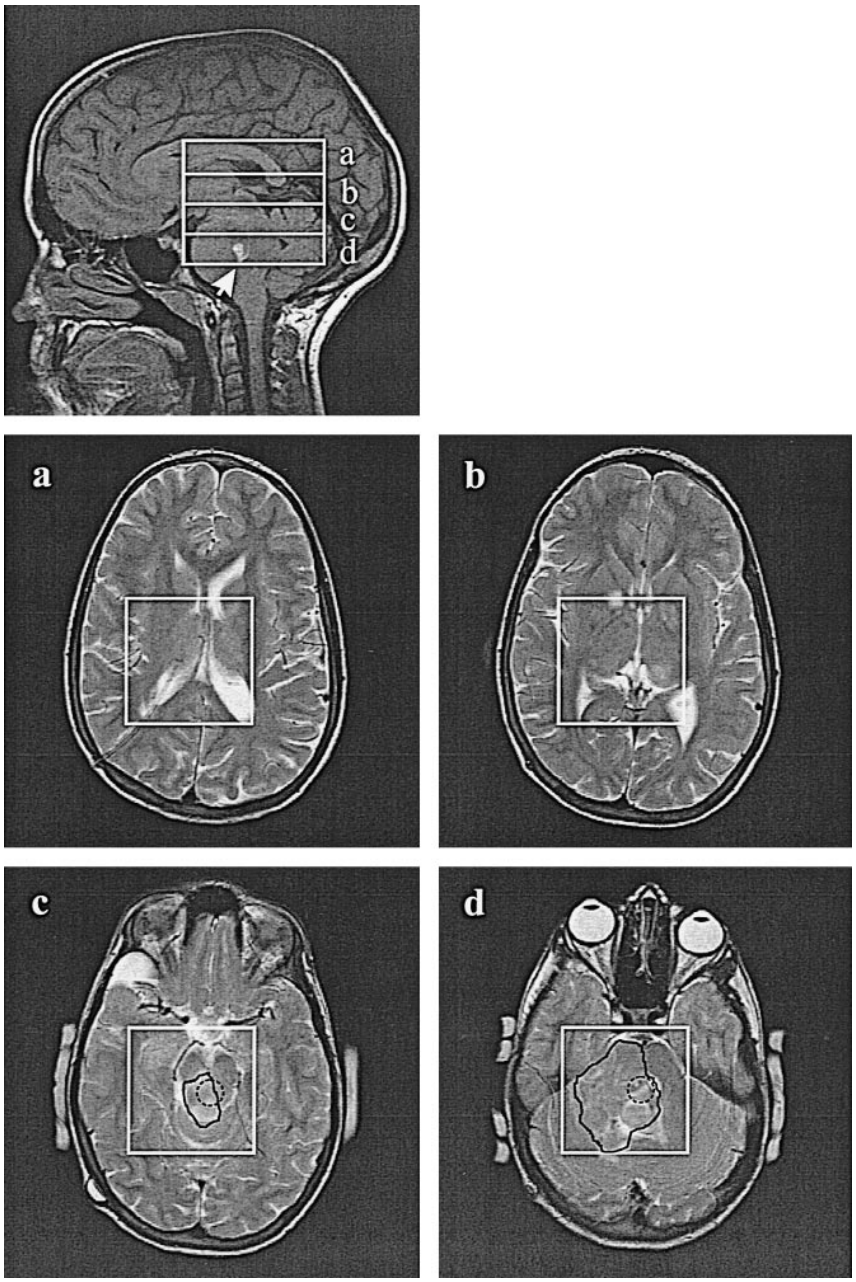

FIG 4. *Top,* Sagittal image superimposed with the 6 × 6 × 6-cm PRESS VOI, the four 1.5-cm-thick HSI slices, *a–d,* and the brain stem glioma in an 11-year-old girl (*arrow*).

a–d, PRESS VOIs and FASI regions are marked with a *solid black line* on the corresponding axial T2-weighted images (FOV = 22 cm) from slices *a–d.* The *dotted circles* on axial images *c* and *d* indicate the location of the glioma.

partial volume effect, since the glioma extends at approximately 45° to the IS axis, as seen on the sagittal image. None of the spectra in Figures 3 or 5 display any lipid or lactate signals upfield from the NAA (2.0–0.5 ppm), indicating the high extraneous fat rejection of the hybrid and the (low) grade of these tumors (29, 30, 32).

The mostly Cho character of the tumor voxel spatially abates rapidly, within a single-voxel step, to a more normal metabolite ratio of approximately 1:1 for Cho:Cr and higher NAA levels, as shown for the healthy control subjects in Figures 6 and 7. An example of the steepness and resolution of the metabolic gradient is indicated by ''G'' in Figure 3d. Cho:Cr decreases from >2, typical of glial tumors (29, 32, 33), to 1.6 and 1.0 within 3 voxels (ie, 2 cm center-to-center). The gradient is steeper in the row of the glioma, where the ratio goes from tumor to normal over a 1-cm step. This behavior is consistent in all directions around the glioma in that figure and is also observed in Figure 5, indicating both the precision and the reproducibility of the 3D methodology.

A voxel Cho:Cr ratio of $\simeq 1$ (SD, σ 0.1) is found in slices that are both tumor and FASI free. This is demonstrated in FASI-free slices in a patient (see Fig 5a and b) and in both control subjects (see Figs 6 and 7). It is also in agreement with the ratio reported elsewhere for healthy adults and children (17, 32–34). Therefore, ''abnormal'' was assigned by moving radially out from the glioma and flagging any voxel whose Cho:Cr ratio was significantly (30%, ie, more than 3σ or $P < .003$) larger than unity and that was

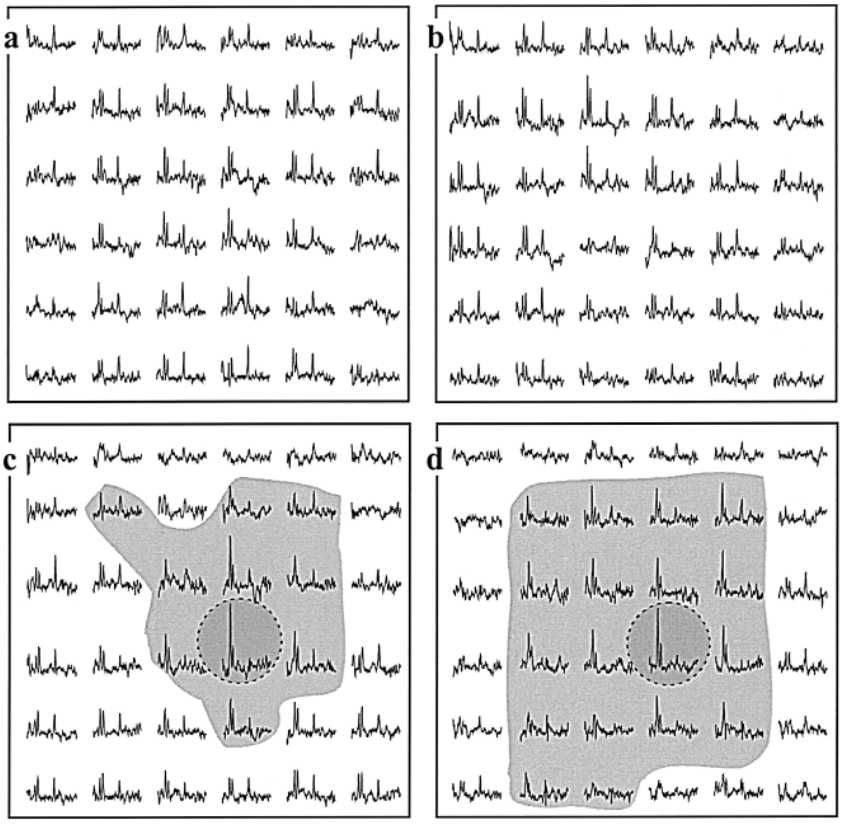

FIG 5. *a–d,* Real part of the proton spectra from the VOIs on the corresponding images in Figure 4. The spectra from the tumor in slices *c* and *d* in the *dashed circle* and regions of elevated 2>Cho:Cr>1.3 are shaded. All spectra display the 4.0 to 0.5 ppm chemical shift range and are plotted on the same vertical scale, and each represents the signal from a 1.5-cm^3 voxel.

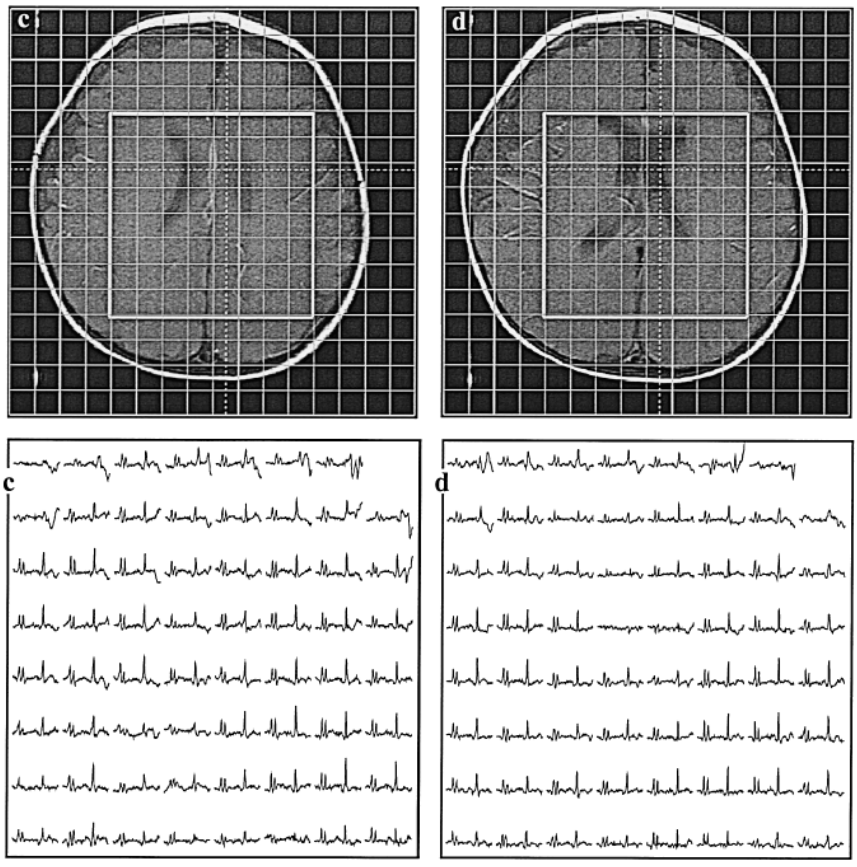

FIG 6. *Top row,* Axial images show the location of the PRESS boxes and 1 × 1-cm CSI grid from the brain of a healthy male 7-month-old control subject, corresponding to the patient in Figures 2c and d and 3c and d.

Bottom row, Real part of the 8 × 8 proton spectra matrices from the corresponding PRESS boxes. Spectra display the 4.0 to 0.5 ppm chemical shift range from each 1-cm^3 voxel and are on a common intensity grid.

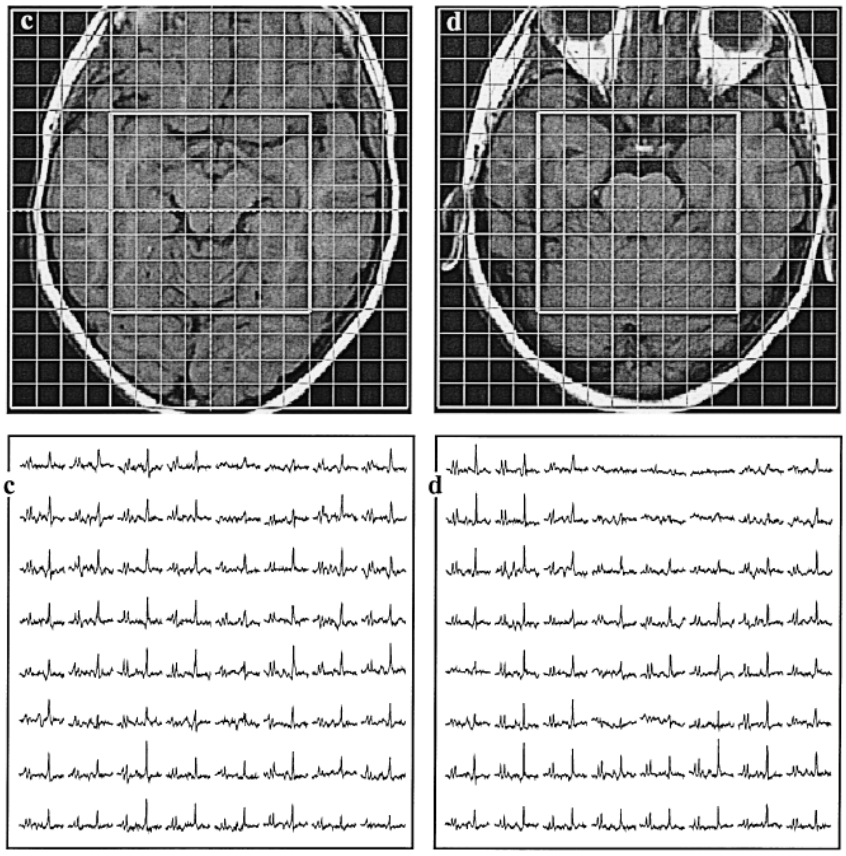

FIG 7. *Top,* Axial images show the location of the PRESS boxes and 1 × 1-cm CSI grid from the brain of a healthy male 11-year-old control subject, corresponding to the patient in Figures 4c and d and 5c and d.

Bottom, Real part of the 8 × 8 proton spectra matrices from the corresponding PRESS boxes. Spectra display the 4.0 to 0.5 ppm chemical shift range from each 1-cm^3 voxel and are on a common intensity grid.

adjacent to at least one other such voxel or to a tumor (ie, a continuity requirement). Subject to these criteria, an entire 3D region surrounding the gliomas is characterized by an elevated Cho:Cr ratio (>1.3) and by nonvanishing levels of NAA, as shown by the shading in Figures 3 and 5. Note that the boundaries of the shaded regions are well defined, owing to the sharp ''normal'' versus ''abnormal'' transitions in that patient. In addition, the Cho:Cr ratio is significantly different in FASI regions as compared with similar regions in control subjects (see Figs 6 and 7).

The extent of these shaded regions of spectra in Figures 3a–d and 5c and d qualitatively overlap with the FASI on the MR images in Figures 2c and d and 4C and D, respectively, but are more extensive. Specifically, the proton MR spectra in Figure 3 indicates a 90-cm^3 (60-voxel) FASI region, whereas the MR images show only about a 45-cm^3 region. For the patient in Figure 5, the MR spectra show a 42-cm^3 (28-voxel) FASI region, but the MR image discloses only about a 26-cm^3 region. Furthermore, the MR spectroscopy abnormality in Figure 3 extends farther in the third dimension, to all four HSI slices, whereas the radiologist identified FASI in only two slices (cf Figs 2 and 3).

The above disparity does not mean that either MR imaging or proton MR spectroscopy is incorrect in estimating the extent of disease, since each imaging technique detects different metabolites: MR imaging shows the water content and the T1 and T2 relaxation properties of the tissue; because of the spongiotic nature of FASI (9), its water level is both elevated and of long T2, leading to the brightness on T2-weighted images. MR spectroscopy, on the other hand, yields the levels of metabolites other than water, and the former need not correlate with the latter. The behavior of these metabolite levels was consistent in all five of our cases and indicated three distinct regions: a) tumor, characterized by high Cho:Cr>2 and no NAA; b) region(s) of elevated, 2>Cho:Cr>1.3; ratio, about a) and partial to full levels of NAA; and c) normal-appearing brain, Cho:Cr $\simeq$ 1 $\pm$ 0.1, at the periphery of b).

The observations a–c are in accordance with those reported recently by Castillo et al (6) using single-voxel proton MR spectroscopy. These authors detected differences between the spectra from the tumor and from the adjoining FASI, the latter being more characteristic of normal brain. They also observed normal-appearing spectra (compared with the same region in the brains of healthy volunteers) outside the FASI in 10 NF1 patients with or without a tumor.

Immunity to Interruption

To reduce the adverse consequence of interruption caused by the patient waking up, the hybrid in Figure 1 was applied in a specific order. The first 6.5-minute acquisition was the one described by the

$i = 1$ row of the fourth-order Hadamard matrix, $\hat{H}_4$, (1111) (17). At its end, 16×16 spectra from the entire VOI were available, but at a fourfold voxel thickness. Next, the $i = 2$ (1–11–1) row was performed, which completed the second-order HSI, doubling the spatial resolution. The $i = 3$ (11–1–1) and $i = 4$ (1–1–11) rows followed, to complete the reconstruction. This approach is necessary, since, unlike Fourier encoding (CSI), HSI has no zero-filling analog. If one or more acquisitions are missing, the reconstruction will generally fail. The above strategy ensures that loss of the third or fourth acquisition will only cost half the spatial resolution in the HSI direction and 40% of the SNR.

This data collection strategy makes the hybrid more immune to interruption than the aggressive four-slice interleaved approach proposed by Duyn and colleagues (14, 15). The latter is based on 128- to 256-millisecond data acquisition periods, short enough to allow interleaving four slices in an overall TR of 2000 and to complete the 3D acquisition in approximately 30 minutes. However, that speed comes at the cost of reduced spectral resolution, owing to the four to eight times shorter signal acquisition time, and to lower immunity, because the four slices are all acquired incrementally, interruption leaves the experimenter with four equally incomplete sets. Since the acquisition of these slices is sparse to begin with, a circular k-space grid, the consequence of such interruption may be total loss of the data. The proposed hybrid does not suffer from either of these two problems.

Conclusion

The HSI-CSI hybrid sequence allows 3D MR spectroscopy in the same amount of time as a 2D acquisition of equal SNR and spatial and spectral resolution. It can be implemented on any imager, since its components, CHESS, OVS, and PRESS, are standard in any spectroscopy package. The method is relatively fast and robust, making this approach well suited for clinical pediatric applications. The clinical findings from these studies indicate that MR spectroscopy of NF1-related optic pathway tumors are distinguished by increased Cho, decreased Cr, and near absence of NAA or lipid signals; FASIs exhibit similar traits, but their NAA level is relatively unchanged compared with normal brain; and normal-appearing regions near the FASI exhibit similar behavior. Therefore, 3D proton MR spectroscopy may distinguish FASIs from either tumor or normal brain tissue and the metabolic abnormality correlates with, but is more extensive than, that indicated by MR imaging.

References

1. Riccardi VM. **Von-Recklinghausen neurofibromatosis.** *N Engl J Med* 1981;305:1617–1627
2. Pont MS, Elster AD. **Lesions of skin and brain: modern imaging of the neurocutaneous syndromes.** *AJR Am J Roentgenol* 1992;158:1193–1203
3. North K, Joy P, Yulle D, et al. **Specific learning disabilities in children with neurofibromatosis type 1: significance of MRI abnormalities.** *Neurology* 1994;44:878–883
4. Moore BDI, Slopis JM, Schomer D, Jackson EF, Levy BM. **Neuropsychological significance of areas of high signal intensity on brain MRIs of children with neurofibromatosis.** *Neurology* 1996;46:1660–1668
5. Joy P, Roberts C, North K, deSilva M. **Neuropsychological function and MRI abnormalities in neurofibromatosis type 1.** *Dev Med Child Neurol* 1995;9:368–377
6. Castillo M, Green C, Kwock L, et al. **Proton MR spectroscopy in patients with neurofibromatosis type 1: evaluation of hamartomas and clinical correlation.** *AJNR Am J Neuroradiol* 1995;16:141–147
7. Molloy PT, Bilaniuk LT, Vaughan SN, et al. **Brainstem tumors in patients with neurofibromatosis type 1: a distinct clinical entity.** *Neurology* 1995;45:1897–1902
8. Castillo M, Kwock L, Green C, Schiro S, Wilson JD, Greenwood R. **Proton MR spectroscopy in a possible enhancing hamartoma in a patient with neurofibromatosis type 1.** *AJNR Am J Neuroradiol* 1995;16:993–996
9. DiPaolo DP, Zimmerman RA, Rorke LB, Zachai EH, Bilaniuk LT, Yachnis AT. **Neurofibromatosis type 1: pathologic substrate of high intensity foci in the brain.** *Radiology* 1995;195:721–724
10. Daston MM, Scrable H, Nordlund M, Sturbaum AK, Nissen LM, Ratner N. **The protein product of the neurofibromatosis type 1 gene is expressed at highest abundance in neurons, schwann cells and oligodendrocytes.** *Neuron* 1992;8:415–428
11. Moonen CTW, Sobering G, van Zijl PCM, Gillen J, von Kienlin M, Bizzi A. **Proton spectroscopic imaging of human brain.** *J Magn Reson* 1992;98:556–575
12. Alger JR, Symko SC, Bizzi A, Posse S, DesPres DJ, Armstrong MR. **Absolute quantitation of short TE brain ^{1}H MR spectra and spectroscopic imaging data.** *J Comput Assist Tomogr* 1993;17:191–199
13. Posse S, Schuknecht B, Smith ME, van Zijl PCM, Herschkowitz N, Moonen CTW. **Short echo time proton MR spectroscopic imaging.** *J Comput Assist Tomogr* 1993;17:1–14
14. Duyn JH, Moonen CTW. **Fast proton spectroscopic imaging of human brain using multiple spin echoes.** *Magn Reson Med* 1993;30:409–414
15. Duyn JH, Gillen J, Sobering G, van Zijl PCM, Moonen CTW. **Multisection proton MR spectroscopic imaging of the brain.** *Radiology* 1993;188:277–282
16. Duijn JH, Matson GB, Maudsley AA, Weiner MW. **3D phase encoding ^{1}H spectroscopic imaging of human brain.** *Magn Reson Imaging* 1992;10:315–319
17. Gonen O, Arias-Mendoza F, Goelman G. **3D localized in vivo ^{1}H spectroscopy of human brain using a hybrid of 1D-Hadamard with 2D-chemical shift imaging.** *Magn Reson Med* 1997;37:644–650
18. Sijens PE, van den Bent MJ, Nowak PJCM, van Dijk P, Oudkerk M. **^{1}H chemical shift imaging reveals loss of brain tumor choline signal after administration of Gd-contrast.** *Magn Reson Med* 1997;37:222–225
19. Gonen O, Hu J, Stoyanova R, Goelman G, Leigh JS, Brown TR. **Hybrid three dimensional (1D-Hadamard, 2D-chemical shift imaging) phosphorus localized spectroscopy of a human brain.** *Magn Reson Med* 1995;33:300–308
20. Gonen O, Murdoch JB, Stoyanova R, Goelman G. **3D multivoxel proton spectroscopy of human brain using a hybrid of 8th-order Hadamard encoding with 2D-chemical shift imaging.** *Magn Reson Med* 1998;38:34–40
21. Dreher W, Leibfritz D. **Double-echo multislice proton spectroscopic imaging using Hadamard slice encoding.** *Magn Reson Med* 1994;31:596–600
22. Bottomley PA. **Spatial localization in NMR spectroscopy in vivo.** *Ann N Y Acad Sci* 1987;508:333–348
23. Gonen O, Hu J, Murphy-Boesch J, et al. **Interleaved heteronuclear (^{1}H-^{31}P) two dimensional chemical shift imaging of in vivo human brain.** *Magn Reson Med* 1994;32:104–109
24. Maudsley AA, Matson GB, Hugg JW, Weiner MW. **Reduced phase encoding in spectroscopic imaging.** *Magn Reson Med* 1994;31:645–651
25. Haase A, Frahm J, Hänicke W, Matthaei D. **^{1}H NMR chemical shift selective (CHESS) imaging.** *Phys Med Biol* 1985;30:341–344
26. Gonen O, Mohebbi A, Stoyanova R, Brown TR. **In vivo phosphorus polarization transfer and decoupling from protons in**

3D localized NMR spectroscopy of human brain. *Magn Reson Med* 1997;37:301–306
27. Toft PB, Christiansen P, Pryds O, Lou HC, Henriksen O. **T1, T2 and concentrations of brain metabolites in neonates and adolescents estimated with H-1 MR spectroscopy.** *J Magn Reson Imaging* 1994;4:1–5
28. Negendank W. **Studies of human tumors by MRS: a review.** *NMR Biomed* 1992;5:303–324
29. Ott D, Henning J, Ernst T. **Human brain tumors: assessment with in vivo proton MR spectroscopy.** *Radiology* 1993;186:745–752
30. Negendank WG, Sauter R. **Intratumoral lipids in ^{1}H MRS in vivo in brain tumors: experience of Siemens cooperative clinical trial.** *Anticancer Res* 1996;16:1533–1538
31. Preul MC, Caramanos Z, Collins DL, et al. **Accurate, noninvasive diagnosis of human brain tumors by using proton magnetic resonance spectroscopy.** *Nat Med* 1996;2:323–326
32. Hagberg G, Burlina AP, Mader I, Roser W, Radue EW, Seelig J. **In vivo proton MR spectroscopy of human gliomas: definition of metabolic coordinates from multidimensional classification.** *Magn Reson Med* 1995;34:242–252
33. Sutton LN, Wang ZJ, Gusnard D, et al. **Proton magnetic resonance spectroscopy of pediatric brain tumors.** *Neurosurgery* 1992;31:195–202
34. Tzika AA, Vigneron DB, Ball WS, Dunn RS, Kirks DR. **Localized proton MR spectroscopy of the brain in children.** *J Magn Reson Imaging* 1993;3:719–729